Materials Today Physics 48 (2024) 101570

Contents lists available at ScienceDirect

Materials Today Physics

journal homepage: www.journals.elsevier.com/materials-today-physics

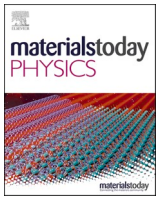

Superior bendability enabled by inherent in-plane elasticity in Bi_2Te_3 thermoelectrics

Yixin Hu [1], Xinyi Shen [1], Zhiwei Chen, Min Liu, Xinyue Zhang, Long Yang, Jun Luo [**], Wen Li [***], Yanzhong Pei [*]

Interdisciplinary Materials Research Center, School of Materials Science and Engineering, Tongji University, 4800 Caoan Rd., Shanghai, 201804, China

A B S T R A C T

With the rapid development of modern wearable electronics, powerful and deformable thermoelectric generators have become an urgent need as the power units that convert environmental or body heat into electricity. Existing efforts mostly focused on the assistance for deformability by substrates/additives, the resultant devices usually output much less power and showed very poor power retainment. Elasticity is inherent to all solids, which therefore offers an intrinsic solution for making thermoelectrics deformable without compromise in power output because of its full recoverability. This work demonstrates this in best-performing $(Bi, Sb)_2(Te, Se)_3$ thermoelectrics near room temperature, ending up in the film devices with both extraordinary power density and robust recoverable bendability. This originates from the inherent large elasticity for the in-plane orientation, which is enabled by an easy tape stripping approach for the Van der Waals layered structure, allowing the realization of both powerfulness and bendability that are equally important for wearable thermoelectrics.

1. Introduction

Thermoelectric as an environment-friendly and silent heat-to-electricity conversion technology, has attracted considerable attention over the decades [1,2]. Particularly in the wake of present explosion of wearable devices, thermoelectricity is urgently needed as a sustainable alternative to electrochemical batteries for continuous powering, utilizing environmental or body heat [3,4]. The challenge largely relies on how to make powerful thermoelectric generators flexible, since known high-performing thermoelectrics are usually fragile inorganics with rigid three-dimensional chemical bonds.

Thermoelectric performance of materials is governed by the material's dimensionless figure of merit $zT = S^2T/\rho\kappa$, where S, T, ρ, and κ are Seebeck coefficient, temperature, electrical resistivity, and thermal conductivity, respectively [5]. For a given temperature difference, the power factor, $PF=S^2/\rho$, becomes the key determining the power output, while zT measures the energy efficiency.

Considering the requirement of flexibility for wearable devices, efforts on developing organic thermoelectrics were initiated a few decades ago [6,7], due to the flexibility of macromolecule chains. Unfortunately, the thermoelectric performance, in particular the power factor of organics ends up being significantly lower than that of inorganics. This further limits a high power output to be achieved, by alternatively compromising the thermoelectric performance and flexibility in inorganics with organic additives [8–10].

Thanks to the periodicity of atomic arrangements in crystalline inorganics, band and transport theories provide clear guidance for optimizing known thermoelectrics and designing new ones. The performance has been improved dramatically in recent decades [11–15], which is also the mainstream of thermoelectric developments in history. However, the inherent rigidity of inorganics largely restricts their applications in flexible scenarios. In fact, there have been so far no report of sufficiently powerful (specific power density >5 μW/cm-K^2) generators allowing recoverable bending for >1000 times [16–20].

Elasticity is inherent to all solid-state materials, which therefore offers a fundamental solution for making thermoelectrics deformable at no explicit expanse of power output because of its full recoverability. In contrast, any plastic deformations challenge the recoverability thus usually induce degradation in functionalities. Geometrically, elastic deformability can be substantially enhanced by thinning the material [21,22], since the minimum bending curvature radius (r_b) is determined by the maximum elastic strain (ε) and the thickness (t) through $r_b = t/2\varepsilon$. For bending radius larger than r_b, the experienced maximum tensile and compressive strains (on the outer and inner surface, respectively) can

* Corresponding author.
** Corresponding author.
*** Corresponding author.
E-mail addresses: junluo@tongji.edu.cn (J. Luo), liwen@tongji.edu.cn (W. Li), yanzhong@tongji.edu.cn (Y. Pei).
[1] These authors contributed equally to this work.

https://doi.org/10.1016/j.mtphys.2024.101570
Received 4 September 2024; Received in revised form 1 October 2024; Accepted 14 October 2024
Available online 16 October 2024

both be ensured to be $<\varepsilon$ for a full recoverability. This is crucial for making functional devices flexible without a degradation in functionality.

As the best-performing thermoelectric material near room temperature, $(Bi, Sb)_2(Te, Se)_3$ alloys differ from others by its layered structure (Fig. S1) [25]. Such a strong structural anisotropy leads to highly directional elastic modulus varying by a factor of ~5 (Fig. 1a and b) between in-plane and out-of-plane directions [23,24], suggesting the existence of a much larger allowed in-plane elastic strain. Note the direction $<\overline{11}\ 20>$ of exactly the best elasticity is about $\pm10^\circ$ for Bi_2Te_3 and $\pm14^\circ$ for Sb_2Te_3 to the basal plane. The strong covalence of in-plane bonds further facilitates a fast charge transport in highly degenerated bands for thermoelectrics [26]. Furthermore, the weak out-of-plane van der Waals bonds provide easy cleavage [25] as in the case of graphite [27]. These features could therefore open a possibility for mechanically stripped single-crystal $(Bi, Sb)_2(Te, Se)_3$ films for powerful and deformable thermoelectric applications (Fig. 1c and d) [28].

Compared to conventional polycrystalline thermoelectric films, stripped single-crystal ones have less imperfection, higher density and higher crystallinity [17,19,29]. In this work, we successfully grew p-type $Bi_{0.5}Sb_{1.5}Te_3$ and n-type $Bi_2Te_{2.88}Se_{0.12}$ single crystals for mechanically stripped films of a typical thickness of ~20 μm for thermoelectric flexible devices [18,19], using polyethylene glycol terephthalate (PET) tapes (Fig. S2). This leads to a successful inheritance of the high in-plane power factor with a big bonus of extraordinary flexibility for recoverably bending for at least 12000 times at a tiny radius of 4 mm. (Fig. 1a).

2. Results and discussion

$Bi_{0.5}Sb_{1.5}Te_3$ and $Bi_2Te_{2.88}Se_{0.12}$ are studied in this work due to their high thermoelectric performance [25] and high inherent in-plane elasticity. According to the phase diagrams (Fig. S3), a vertical gradient freeze (VGF) technique with a small temperature gradient of 8 K/cm at a cooling rate of ~2 K/h leads to a successful growth of homogenous $Bi_{0.5}Sb_{1.5}Te_3$ and $Bi_2Te_{2.88}Se_{0.12}$ single crystals (Fig. 1c). The much smaller temperature gradient here is used to reduce the driven force of nucleation [30] and VGF technique enables a removal of motions, both of which are important to ensure less imperfections as compared to the case of Bridgman technique [28]. More details of the single-crystal growth are introduced in the Supplementary. The X-ray diffraction (XRD) patterns of the typical cleavage surfaces at room temperature reveal the preferred crystallographic orientation along the out-of-plane direction (Fig. 2a and b). The composition dependent lattice parameters suggest the formation of single crystals with the desired composition (Fig. S4).

The cleavability of the single-crystal bulks can be understood by the weak van der Waals bonds [31] between (0001) quintuple layers. This further facilitates an easy stripping for films with thickness down to 20

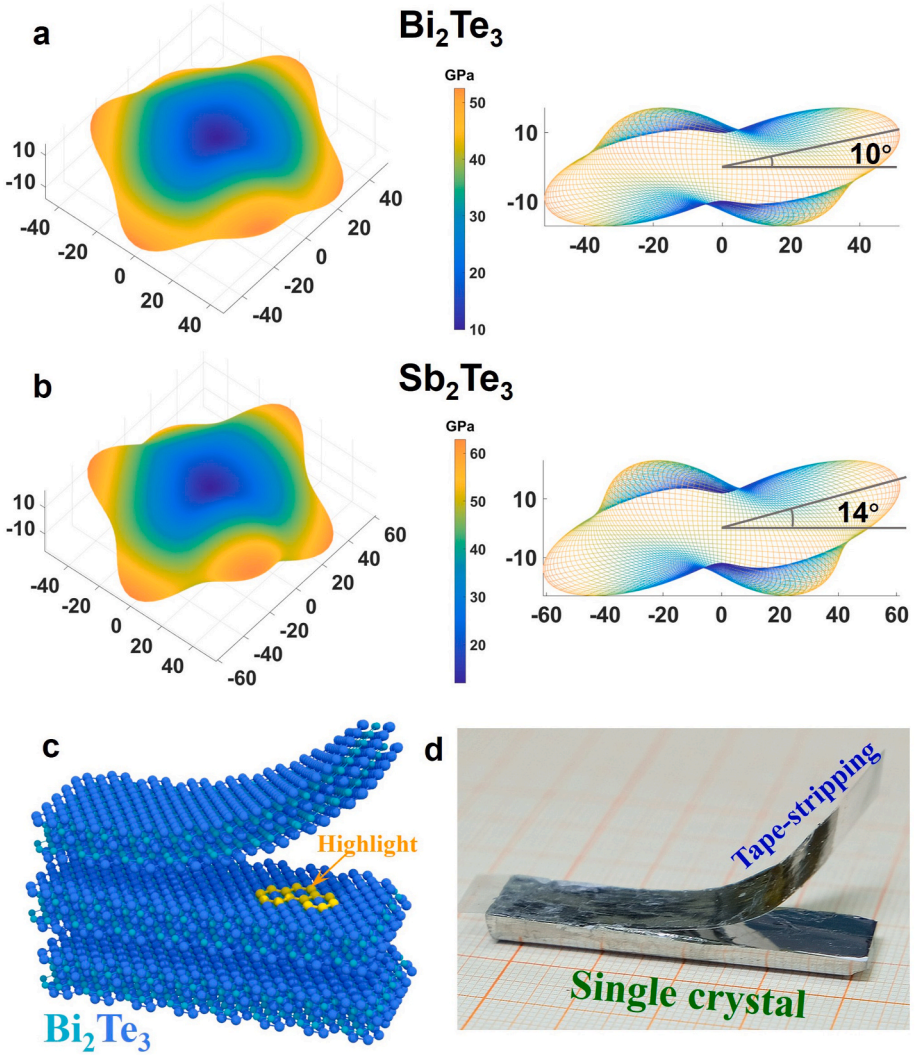

Fig. 1. Elasticity and cleavage. Calculated [23,24] full-space mapping on elastic modulus and the corresponding two-dimensional contours for Bi_2Te_3 (a) and Sb_2Te_3 (b). Schematic crystal structure of Bi_2Te_3 (c) and photograph of $Bi_{0.5}Sb_{1.5}Te_3$ single crystal during tape-stripping (d).

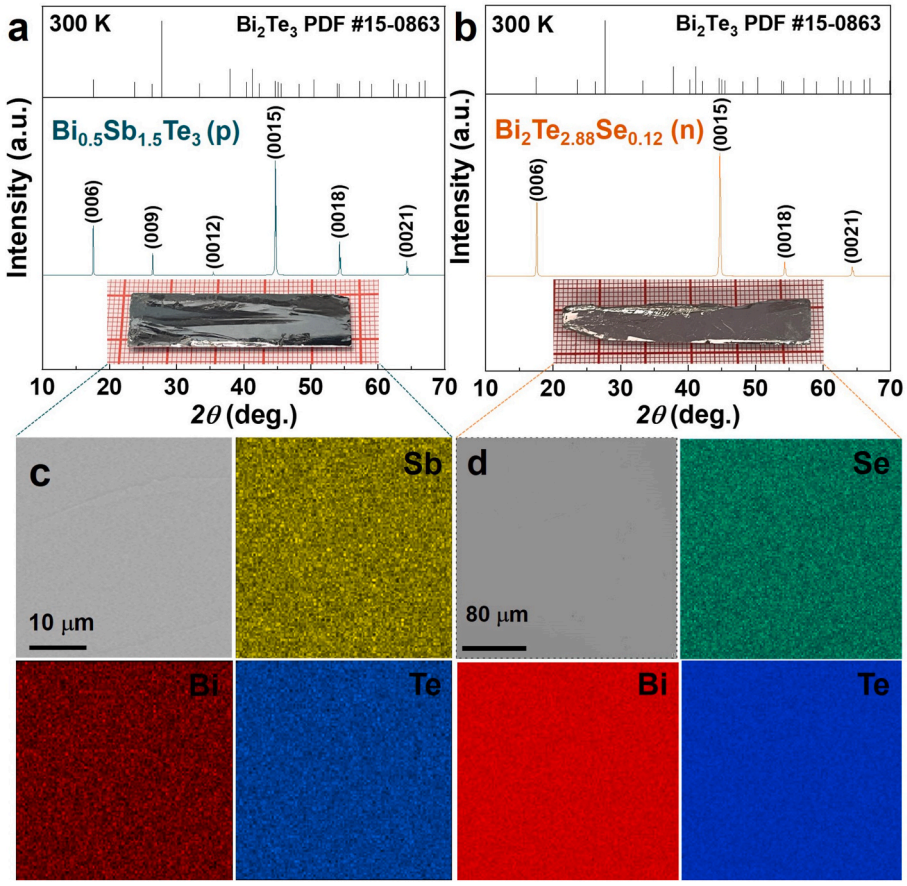

Fig. 2. Phase composition. XRD patterns to the typical cleavage surfaces of the (001) plane (a, b) and SEM images with corresponding EDS mappings (c, d) for $Bi_{0.5}Sb_{1.5}Te_3$ (a, c) and $Bi_2Te_{2.88}Se_{0.12}$ (b, d).

μm using PET tapes (Figs. S5–S6). Scanning electron microscopy (SEM) images and the corresponding energy dispersive spectroscopy (EDS) mappings indicate the homogeneity and high density of single-crystal films (Fig. 2c and d). Importantly, such films exhibit exceptional bendability at a curvature radius down to 4 mm, meeting the requirements of wearable thermoelectrics using body heat.

Superior in-plane thermoelectric performance is secured in anisotropically structured $(Bi, Sb)_2(Te, Se)_3$ alloys [25,32]. The details of the transport properties for both single-crystalline bulks and films are shown in Fig. 3 and Figs. S7–S8. Moreover, carrier concentration dependent Seebeck coefficient (Fig. 3c) and Hall mobility (μ_H) (Fig. 3d) for single crystals in this work, show very good agreements with literature results for single crystals [33–44]. The power factor of both single-crystal films here are much higher than the majority of the reported flexible films (Fig. 3e and f) [17–19,31,45–56].

Note the above discussion is based on the intrinsic transport behaviors in $(Bi, Sb)_2(Te, Se)_3$ alloys. More recently, He et al. [28] reported the thermoelectric properties of $(Bi, Sb)_2(Te, Se)_3$ films, where a Bridgman technique was used to grow the single crystals. Obvious extrinsic transport behavior can be observed, for instance, the resultant staggered-layer defects [28] largely led to an increase in carrier concentration but a decrease in mobility. In addition, staggered-layer defects lead to an increase in Seebeck coefficient. In this work, the electronic transport properties of films are nearly intrinsic, which are all quite comparable to those of bulks and consistent with most of literature results, indicating the absence in stripped films of staggered-layer defects. This may further help understand the difference in bending recoverability in this work, since the staggered-layer defects may promote extrinsic stress propagation [28]. Note that Se-alloying results in a significant reduction of Hall mobility for the obtained n-type samples due to the additional carrier scattering and increased band effective mass induced by the Te/Se substitutional point defects [57] and band gap broadening [58], respectively (Fig. 3d).

Powerful thermoelectric generators require not only high-performance materials, but also conductive contacts. Previous works [16,49,59] on film generators usually use silver paste to glue the thermoelectric materials and electrodes, leaving a large room for further improvements. In this work, the Ga-In liquid alloy with a melting point of 288 K [60] is used to fuse the thermoelectric films and 0.01-mm-thick silver foil electrodes with a coverage of polyethylene terephthalate/ethylene-vinyl acetate copolymers for protection. The Ga-In alloy acts as a wetting layer, ensuring a tighter and more uniform contact between the silver foil electrode and the thermoelectric films, which significantly reduces the contact resistance. Additionally, the use of the encapsulation film further improves the adhesion between the silver foil and the film, forming a better Ohmic contact and contributing to the low internal resistance. The internal resistances (R_{in}) for p-type $Bi_{0.5}Sb_{1.5}Te_3$ and n-type $Bi_2Te_{2.88}Se_{0.12}$ single-leg film devices, with the sizes of ~$8 \times 3 \times 0.02$ mm^3 and ~$7 \times 4 \times 0.02$ mm^3, respectively, were measured by the four-probe technique (Fig. S9) across the contacts along multiple parallel paths for averaging (Fig. 4a). The corresponding interfacial contact resistivities (ρ_c) for both films here are estimated to be only ~1.34 mΩ cm^2 (p-type) and 1.24 mΩ cm^2 (n-type), which are significantly lower than that reported in the literature (Table S2).

A four-leg thermoelectric generator (Fig. S10) assembled by two pairs of $Bi_{0.5}Sb_{1.5}Te_3$ ($20 \times 6 \times 0.022$ mm^3) and $Bi_2Te_{2.88}Se_{0.12}$ ($20 \times 6 \times 0.02$ mm^3) single-leg devices, shows powerful outputs (Fig. 4c). At a fixed cold-side temperature (T_c) of ~300 K during the measurement, a larger temperature difference (ΔT) leads to a higher open-circuit voltage (V_{oc}), which is comparable to the prediction according to the

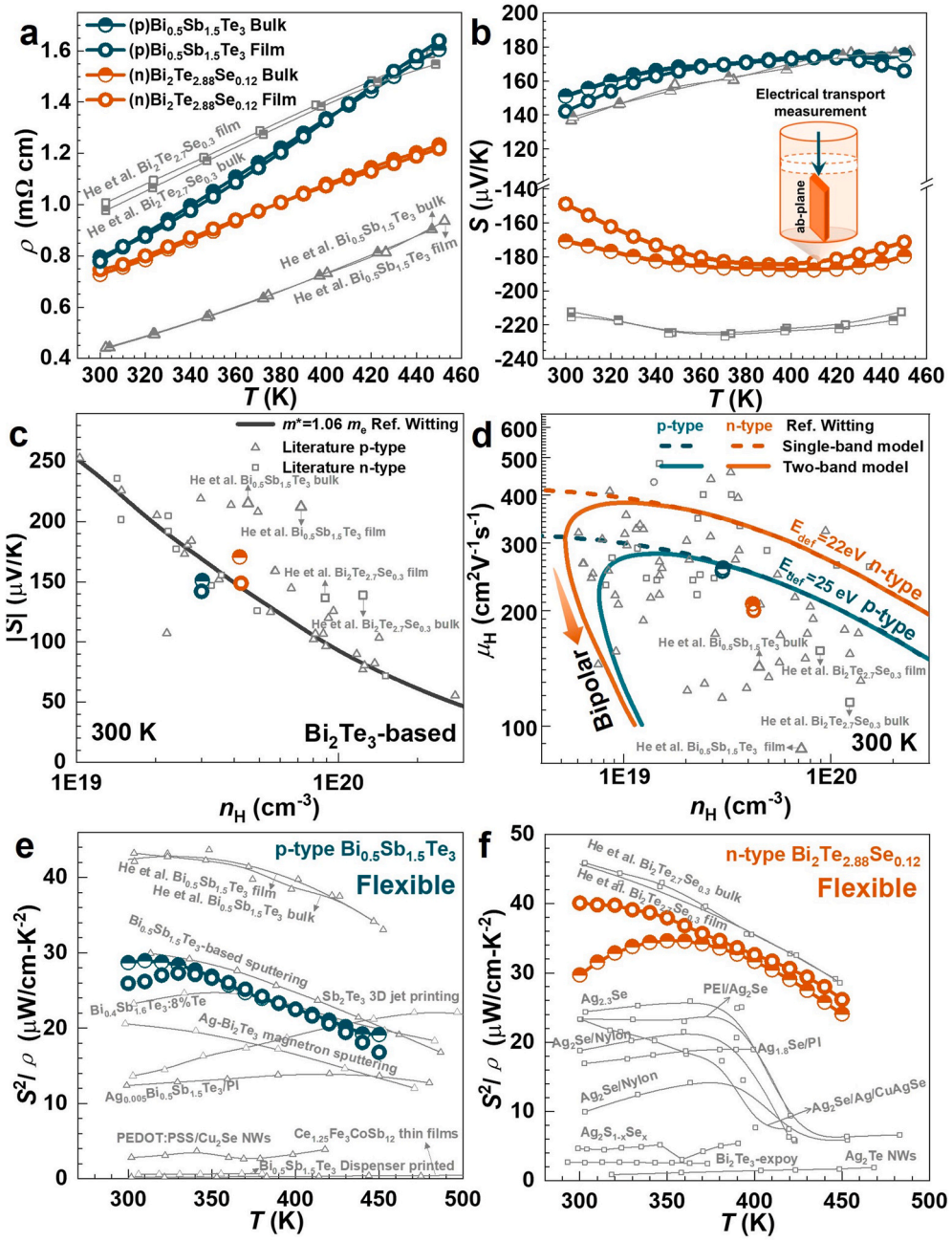

Fig. 3. Thermoelectric properties. Temperature dependent in-plane electrical resistivity (a) and Seebeck coefficient (b), room temperature Hall carrier concentration (n_H) dependent Seebeck coefficient (c) and Hall mobility (μ_H) (d), and temperature dependent power factor (S^2/ρ) (e, f) for $Bi_{0.5}Sb_{1.5}Te_3$ (e) and $Bi_2Te_{2.88}Se_{0.12}$ (f), with a comparison to the literature results for flexible thermoelectric generators. Literature results of single crystal in (c) and (d) from Refs. [28,33–44] and single-band and two-band model predictions from Ref. [26] are included for comparison.

temperature dependent Seebeck coefficient (Fig. S11a). Additionally, the measured R_{in} well follows the prediction according to the temperature dependent resistivity due to the low ρ_c achieved here (Fig. S11b). As a result, a maximum P^{max} up to 273 μW is realized at ΔT of ~106 K (Fig. 4c), corresponding to a maximum power density (P_d^{max}) of 517 W/m^2 estimated by dividing the power by the cross-section area of thermoelectric materials. Note that the maximum power density in this work is revealed to be one of the highest for polycrystalline flexible generators in the whole range of ΔT interested for wearable electronics (Fig. 4d) [17–19,28,31,46–53,55,56,61–72]. Further taking into account the effect of leg's length, the specific power density ($P_d^{max}L/\Delta T^2$) enables a full measure of output capability among generators of any materials, size and ΔT. The superiority of the generators in this work is further ensured by the higher specific power density as compared to literature results (Fig. S11d) [17,18,45–48,50,52,53,64,66,71].

The single-leg devices and generators simultaneously show extraordinary flexibility (Fig. 5) as confirmed by the excellent recoverability in properties including relative resistance ($R/R_{initial}$), Seebeck coefficient ($S/S_{initial}$) and power factor ($PF/PF_{initial}$), with a large number of bending at a small radius of 4 mm (Fig. S12). The elastic strain for both p- and n-type Bi_2Te_3-based thermoelectrics has been revealed to be higher than 0.3 % based on the mechanical test of three-point bending [73], which is larger than the needed strain of ~0.25 % ($=t/2r_b$ with a bending radius of r_b and a thickness of t) for the elastic bending of the ~20 μm thick film at a radius of 4 mm, ensuring the preservation of nearly constant transport properties. This work enables a much better bending stability

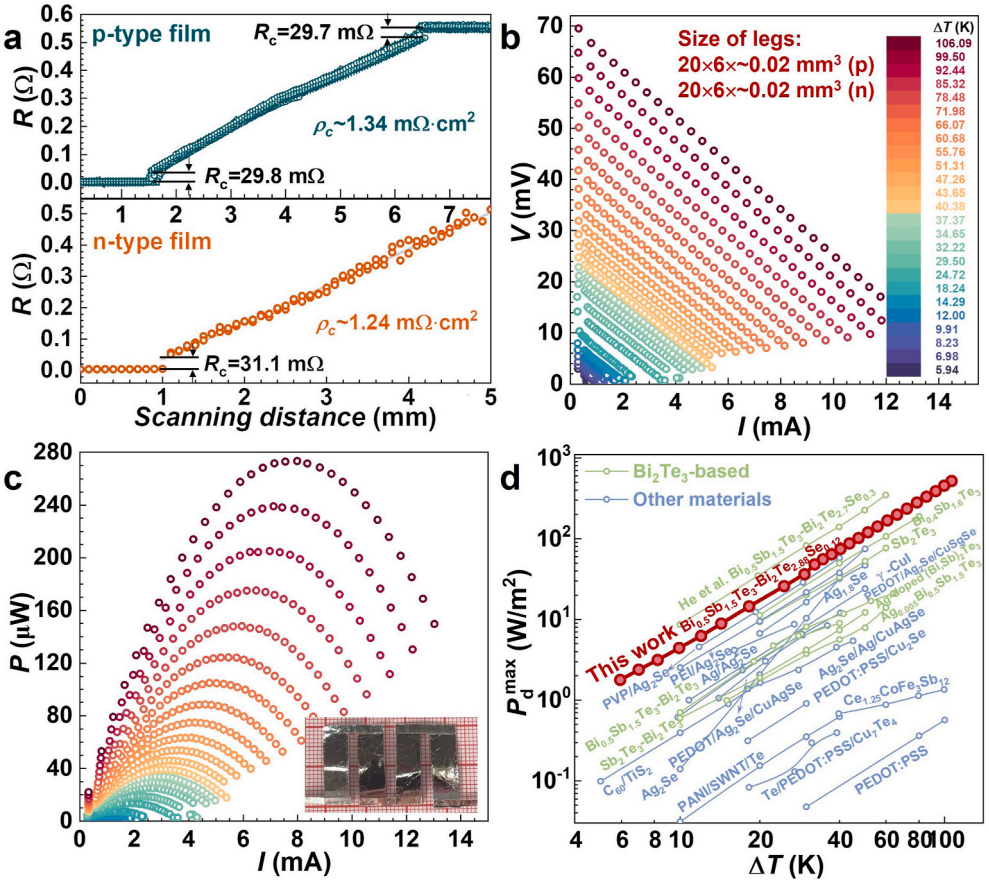

Fig. 4. Interfacial contact resistance and power output. The internal resistance (R_{in}) versus scanning position (a) for p-type $Bi_{0.5}Sb_{1.5}Te_2$ and n-type $Bi_2Te_{2.88}Se_{0.12}$ single-leg devices, output voltage (V, b) and output power (P, c) versus load current (I) at various temperature differences (ΔT), and maximum power density (P_d^{max}) versus ΔT for a four-leg flexible generator with a comparison to literature results of flexible generators [17–20,28,31,46–53,55,56,61–72] (d).

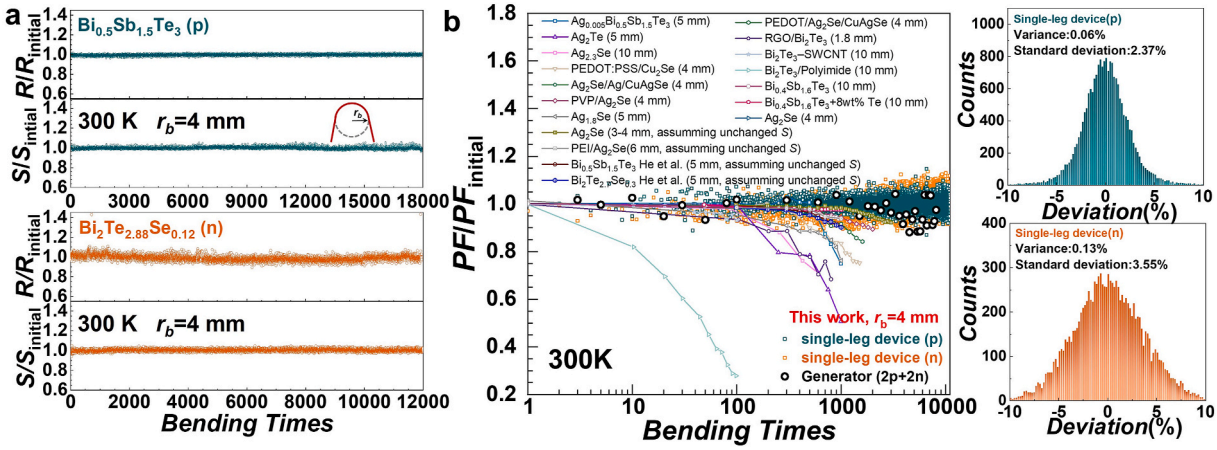

Fig. 5. Flexibility. Relative resistance ($R/R_{initial}$) and relative Seebeck coefficient ($S/S_{initial}$) as a function of bending times for p-type $Bi_{0.5}Sb_{1.5}Te_2$ and n-type $Bi_2Te_{2.88}Se_{0.12}$ films (a). The relative power factor ($PF/PF_{initial}$) as a function of bending times with a statistical analysis and a comparison to that of literature results [18,20,28,46–51,54,56,59,63,74] (b).

than existing ones [18,46–51,54,56,59,63,74], due to the excellent inherently in-plane elasticity.

3. Conclusions

The single-crystal $Bi_{0.5}Sb_{1.5}Te_3$ and $Bi_2Te_{2.88}Se_{0.12}$ films are successfully tape-stripped from bulks as they are structured with weak out-of-plane van der Waals bonds. Due to the inherent large in-plane elasticity, the fabricated flexible thermoelectric generators of single-crystal films enable the first realization of both powerfulness and bendability. The fast in-plane charge transport and large elasticity are common features for layer-structured crystals, therefore the strategy of inherent elasticity is promising to open new possibilities of functional devices with built-in flexibility.

CRediT authorship contribution statement

Yixin Hu: Writing – original draft, Visualization, Project administration, Methodology, Investigation, Formal analysis, Data curation. **Xinyi Shen:** Visualization, Methodology, Investigation, Formal analysis. **Zhiwei Chen:** Writing – review & editing, Funding acquisition, Formal analysis. **Min Liu:** Methodology, Investigation. **Xinyue Zhang:** Methodology, Investigation. **Long Yang:** Methodology, Investigation. **Jun Luo:** Writing – review & editing, Formal analysis, Conceptualization. **Wen Li:** Writing – review & editing, Writing – original draft, Visualization, Validation, Supervision, Resources, Project administration, Methodology, Investigation, Funding acquisition, Formal analysis, Conceptualization. **Yanzhong Pei:** Writing – review & editing, Visualization, Validation, Supervision, Resources, Project administration, Methodology, Investigation, Funding acquisition, Formal analysis, Conceptualization.

Declaration of competing interest

The authors declare that they have no known competing financial interests or personal relationships that could have appeared to influence the work reported in this paper.

Acknowledgements

This work is supported by the National Key Research and Development Program of China (2023YFB3809400), the National Natural Science Foundation of China (Grant No. T2125008, 92163203, 52371234 and 92263108), the Innovation Program of Shanghai Municipal Education Commission (2021-01-07-00-07-E00096) and the Hong Kong, Macao and Taiwan Science and Technology Cooperation Project for Science and Technology Innovation Plan of Shanghai (23520760600).

Appendix A. Supplementary data

Supplementary data to this article can be found online at https://doi.org/10.1016/j.mtphys.2024.101570.

Data availability

Data will be made available on request.

References

[1] B. L. E., Cooling, heating, generating power, and recovering waste heat with thermoelectric systems, Science 321 (2008) 1457–1461.
[2] Z. X, B. Z, S. X, Electronic quality factor for thermoelectrics, Sci. Adv. 6 (2020): eabc0726.
[3] T.E.S. Snyder G J, Complex thermoelectric materials, Nat. Mater. 7 (2008) 105–114.
[4] F. Suarez, A. Nozariasbmarz, D. Vashaee, M.C. Öztürk, Designing thermoelectric generators for self-powered wearable electronics, Energy Environ. Sci. 9 (2016) 2099–2113.
[5] A.F. Ioffe, et al., Semiconductor thermoelements and thermoelectric cooling, Phys. Today 12 (1959) 42.
[6] C. Wan, et al., Flexible n-type thermoelectric materials by organic intercalation of layered transition metal dichalcogenide TiS_2, Nat. Mater. 14 (2015) 622–627.
[7] O. Bubnova, et al., Optimization of the thermoelectric figure of merit in the conducting polymer poly(3,4-ethylenedioxythiophene), Nat. Mater. 10 (2011) 429–433.
[8] Y. Wang, et al., Flexible thermoelectric materials and generators: challenges and innovations, Adv. Mater. (Weinheim, Ger.) 31 (2019): e1807916.
[9] H. Wang, et al., Thermally driven large N-type voltage responses from hybrids of carbon nanotubes and poly(3,4-ethylenedioxythiophene) with tetrakis (dimethylamino)ethylene, Adv. Mater. (Weinheim, Ger.) 27 (2015) 6855–6861.
[10] Q. Yao, Q. Wang, L. Wang, L. Chen, Abnormally enhanced thermoelectric transport properties of SWNT/PANI hybrid films by the strengthened PANI molecular ordering, Energy Environ. Sci. 7 (2014) 3801–3807.
[11] Y. Pei, et al., Convergence of electronic bands for high performance bulk thermoelectrics, Nature 473 (2011) 66–69.
[12] W. Liu, et al., Convergence of conduction bands as a means of enhancing thermoelectric performance of n-type $Mg_2Si_{1-x}Sn_x$ solid solutions, Phys. Rev. Lett. 108 (2012): 166601.
[13] Z. Chen, X. Zhang, Y. Pei, Manipulation of phonon transport in thermoelectrics, Adv. Mater. (Weinheim, Ger.) 30 (2018): e1705617.
[14] K.-J. Liu, et al., Entropy engineering in CaZn2Sb2–YbMg2Sb2 Zintl alloys for enhanced thermoelectric performance, Rare Met. 41 (2022) 2998–3004.
[15] H.-X. Liu, X.-Y. Zhang, Z.-L. Bu, W. Li, Y.-Z. Pei, Thermoelectric properties of (GeTe)1-x[(Ag2Te)0.4(Sb2Te3)0.6]x alloys, Rare Met. 41 (2021) 921–930.
[16] Y. Lei, et al., Microstructurally tailored thin beta-Ag_2Se films towards commercial flexible thermoelectrics, Adv. Mater. (Weinheim, Ger.) (2021): e2104786, https://doi.org/10.1002/adma.202104786.
[17] Y. Ding, et al., High performance n-type Ag_2Se film on nylon membrane for flexible thermoelectric power generator, Nat. Commun. 10 (2019) 841.
[18] T. Varghese, et al., Flexible thermoelectric devices of ultrahigh power factor by scalable printing and interface engineering, Adv. Funct. Mater. 30 (2019).
[19] Z.-H. Zheng, et al., Harvesting waste heat with flexible Bi_2Te_3 thermoelectric thin film, Nat. Sustainability 6 (2022) 180–191.
[20] Y. Liu, et al., Fully inkjet-printed Ag_2Se flexible thermoelectric devices for sustainable power generation, Nat. Commun. 15 (2024) 2141.
[21] W. Liu, et al., Flexible solar cells based on foldable silicon wafers with blunted edges, Nature 617 (2023) 717–723.
[22] J. Pelleg, Mechanical Properties of Materials, vol. 190, Springer, 2013.
[23] Anonymous (Materials Project for Bi_2Te_3 (mp-34202). in https://next-gen.materialsproject.org/materials/mp-34202?chemsys=Bi-Te.
[24] Anonymous (Materials Project for Sb_2Te_3 (mp-1201) in https://next-gen.materialsproject.org/materials/mp-1201?chemsys=Sb-Te.
[25] H.J. Goldsmid, Introduction to Thermoelectricity, vol. 121, Springer, 2010.
[26] I.T. Witting, et al., The thermoelectric properties of bismuth telluride, Adv. Electron. Mater. 5 (2019): 1800904.
[27] G. A. K., Graphene: status and prospects, Science 324 (2009) 1530–1534.
[28] Y. Lu, et al., Staggered-layer-boosted flexible Bi_2Te_3 films with high thermoelectric performance, Nat. Nanotechnol. 18 (2023) 1281–1288.
[29] Q. Jin, et al., Flexible layer-structured Bi_2Te_3 thermoelectric on a carbon nanotube scaffold, Nat. Mater. 18 (2019) 62–68.
[30] W.A. Gault, E.M. Monberg, J.E. Clemans, A novel application of the vertical gradient freeze method to the growth of high quality III–V crystals, J. Cryst. Growth 74 (1986) 491–506.
[31] H. Shang, et al., $Bi_{0.5}Sb_{1.5}Te_3$-based films for flexible thermoelectric devices, J. Mater. Chem. A 8 (2020) 4552–4561.
[32] H.J. Goldsmid, Recent studies of bismuth telluride and its alloys, J. Appl. Phys. 32 (1961) 2198–2202.
[33] V.S. Gaidukova, R.S. Erofeev, V.N. Ovechkina, Peculiarities of energy spectrum of solid solutions in Sb_2Te_3-Bi_2Te_3 system, Izv. Akad. Nauk SSSR, Neorg. Mater.; (USSR), Medium: X (1981) 244–247. Size.
[34] M. Stordeur, M. Stölzer, H. Sobotta, V. Riede, Investigation of the valence band structure of thermoelectric $(Bi_{1-x}Sb_x)_2Te_3$ single crystals, Phys. Status Solidi B 150 (1988) 165–176.
[35] J. Jiang, L. Chen, S. Bai, Q. Yao, Q. Wang, Thermoelectric properties of p-type $(Bi_2Te_3)_x(Sb_2Te_3)_{1-x}$ crystals prepared via zone melting, J. Cryst. Growth 277 (2005) 258–263.
[36] Č. Drašar, et al., Figure of merit of quaternary $(Sb_{0.75}Bi_{0.25})_{2-x}In_xTe_3$ single crystals, J. Appl. Phys. 104 (2008).
[37] V.A. Kulbachinskii, A.V.G. Kytin, P.M. Tarasov, Fermi surface and thermoelectric power of $(Bi_{1-x}Sb_x)_2Te_3$ single crystals doped by Ag, Sn, Ga, IEEE (2006) 459–464.
[38] C.M. Jaworski, V. Kulbachinskii, J.P. Heremans, Resonant level formed by tin in Bi_2Te_3 and the enhancement of room-temperature thermoelectric power, Phys. Rev. B 80 (2009).
[39] B. U, Untersuchung der intermetallischen Verbindung Bi_2Te_3 sowie der festen Lösungen $Bi_{2-x}Sb_xTe_3$ und $Bi_2Te_{3-x}Se_x$ hinsichtlich ihrer Eignung als Material für Halbleiter-Thermoelemente, Z. Naturforsch. 13 (1958) 780–792.
[40] T. Plecháček, J. Navrátil, J. Horák, P. Lošťák, Defect structure of Pb-doped Bi_2Te_3 single crystals, Phil. Mag. 84 (2004) 2217–2228.
[41] J. Bludská, I. Jakubec, Č. Drašar, P. Lošťák, J. Horák, Structural defects in Cu-doped Bi_2Te_3 single crystals, Phil. Mag. 87 (2007) 325–335.
[42] J.N. til, I. Klichova, S. Karamazov, J.S. m, J.H. k, Behavior of Ag admixtures in Sb_2Te_3 and Bi_2Te_3 single crystals, J. Solid State Chem. 140 (1998) 29–37.
[43] Z. M. K, N. S. A, S. T. E., Specific features of Bi_2Te_3 doping with Sn, Phys. Solid State 40 (1998) 1297–1300.
[44] M. R, W. W, The electrical properties of bismuth telluride, Proc. Phys. Soc. 72 (1958) 733.
[45] C. Dun, et al., 3D printing of solution-processable 2D nanoplates and 1D nanorods for flexible thermoelectrics with ultrahigh power factor at low-medium temperatures, Adv. Sci. 6 (2019): 1901788.
[46] H. Shang, et al., High-performance Ag-modified $Bi_{0.5}Sb_{1.5}Te_3$ films for the flexible thermoelectric generator, ACS Appl. Mater. Interfaces 12 (2020) 7358–7365.
[47] Y. Lu, et al., Good performance and flexible PEDOT:PSS/Cu_2Se nanowire thermoelectric composite films, ACS Appl. Mater. Interfaces 11 (2019) 12819–12829.
[48] J. Gao, et al., Thermoelectric flexible silver selenide films: compositional and length optimization, iScience 23 (2020): 100753.
[49] Y. Lu, et al., Ultrahigh power factor and flexible silver selenide-based composite film for thermoelectric devices, Energy Environ. Sci. 13 (2020) 1240–1249.
[50] C. Jiang, et al., Ultrahigh performance of n-type Ag_2Se films for flexible thermoelectric power generators, ACS Appl. Mater. Interfaces 12 (2020) 9646–9655.

[51] S. Hou, et al., High performance wearable thermoelectric generators using Ag_2Se films with large carrier mobility, Nano Energy 87 (2021).
[52] M. Wu, et al., High thermoelectric performance and ultrahigh flexibility $Ag_2S_{1-x}Se_x$ film on a nylon membrane, ACS Appl. Mater. Interfaces 15 (2023) 8415–8423.
[53] D. Madan, et al., Enhanced performance of dispenser printed MA n-type Bi_2Te_3 composite thermoelectric generators, ACS Appl. Mater. Interfaces 4 (2012) 6117–6124.
[54] J. Gao, et al., A novel glass-fiber-aided cold-press method for fabrication of n-type Ag_2Te nanowires thermoelectric film on flexible copy-paper substrate, J. Mater. Chem. A 5 (2017) 24740–24748.
[55] D. Li, et al., High-performance flexible p-type Ce-filled Fe3CoSb12 skutterudite thin film for medium-to-high-temperature applications, Nat. Commun. 15 (2024).
[56] Q.X. Hu, et al., Carrier separation boosts thermoelectric performance of flexible n-type Ag2Se-based films, Adv. Energy Mater. (2024): 202401890, https://doi.org/10.1002/aenm.
[57] R.-S. Zhai, T.-J. Zhu, Improved thermoelectric properties of zone-melted p-type bismuth-telluride-based alloys for power generation, Rare Met. 41 (2022) 1490–1495.
[58] T. Fang, et al., Complex band structures and lattice dynamics of Bi2Te3-based compounds and solid solutions, Adv. Funct. Mater. 29 (2019).
[59] C. Jiang, et al., Ultrahigh performance polyvinylpyrrolidone/Ag_2Se composite thermoelectric film for flexible energy harvesting, Nano Energy 80 (2021): 105488.
[60] J.P. Denny, J.H. Hamilton, J.R. Lewis, Constitution of the system gallium-indium, The Journal of The Minerals 4 (1952) 39–42.
[61] D. Madan, et al., Dispenser printed circular thermoelectric devices using Bi and $Bi_{0.5}Sb_{1.5}Te_3$, Appl. Phys. Lett. 104 (2014).
[62] A. Chen, D. Madan, P.K. Wright, J.W. Evans, Dispenser-printed planar thick-film thermoelectric energy generators, J. Micromech. Microeng. 21 (2011).
[63] Y. Lu, et al., Ultrahigh performance PEDOT/Ag_2Se/CuAgSe composite film for wearable thermoelectric power generators, Materials Today Physics 14 (2020).
[64] J.H. We, S.J. Kim, B.J. Cho, Hybrid composite of screen-printed inorganic thermoelectric film and organic conducting polymer for flexible thermoelectric power generator, Energy 73 (2014) 506–512.
[65] J.P. Rojas, et al., Paper-based origami flexible and foldable thermoelectric nanogenerator, Nano Energy 31 (2017) 296–301.
[66] Q. Gao, et al., High power factor Ag/Ag_2Se composite films for flexible thermoelectric generators, ACS Appl. Mater. Interfaces 13 (2021) 14327–14333.
[67] Y. Du, et al., Multifold enhancement of the output power of flexible thermoelectric generators made from cotton fabrics coated with conducting polymer, RSC Adv. 7 (2017) 43737–43742.
[68] C. Li, et al., A simple thermoelectric device based on inorganic/organic composite thin film for energy harvesting, Chem. Eng. J. (Lausanne) 320 (2017) 201–210.
[69] P. Li, et al., Facile green strategy for improving thermoelectric performance of carbon nanotube/polyaniline composites by ethanol treatment, Compos. Sci. Technol. 189 (2020).
[70] M. Hokazono, H. Anno, N. Toshima, Thermoelectric properties and thermal stability of PEDOT:PSS films on a polyimide substrate and application in flexible energy conversion devices, J. Electron. Mater. 43 (2014) 2196–2201.
[71] L. Wang, et al., Solution-printable fullerene/TiS_2 organic/inorganic hybrids for high-performance flexible n-type thermoelectrics, Energy Environ. Sci. 11 (2018) 1307–1317.
[72] C. Yang, et al., Transparent flexible thermoelectric material based on non-toxic earth-abundant p-type copper iodide thin film, Nat. Commun. 8 (2017): 16076.
[73] M. Liu, X. Zhang, S. Zhang, Y. Pei, Ag_2Se as a tougher alternative to n-type Bi_2Te_3 thermoelectrics, Nat. Commun. 15 (2024) 6580.
[74] B. Wu, et al., High-performance flexible thermoelectric devices based on all-inorganic hybrid films for harvesting low-grade heat, Adv. Funct. Mater. 29 (2019): 1900304.